Journal Pre-proofs

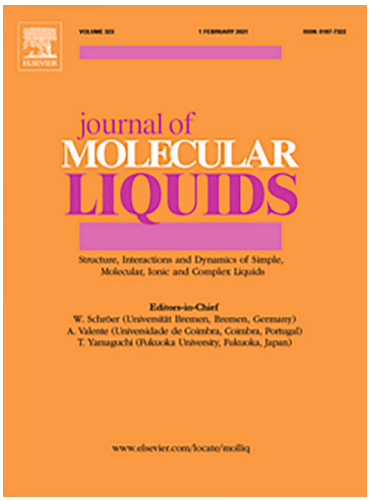

Electric-field-induced patterns in a hockey-stick nematic

Jun Zhang, Ying Xiang, Xiaoyu Ding, Luguo Hao, Supreet Kaur, Golam Mohiuddin, Santanu Kumar Pal, Péter Salamon, Nándor Éber, Ágnes Buka

PII: S0167-7322(22)01778-0
DOI: https://doi.org/10.1016/j.molliq.2022.120239
Reference: MOLLIQ 120239

To appear in: *Journal of Molecular Liquids*

Received Date: 31 March 2022
Revised Date: 8 August 2022
Accepted Date: 27 August 2022

Please cite this article as: J. Zhang, Y. Xiang, X. Ding, L. Hao, S. Kaur, G. Mohiuddin, S. Kumar Pal, P. Salamon, N. Éber, A. Buka, Electric-field-induced patterns in a hockey-stick nematic, *Journal of Molecular Liquids* (2022), doi: https://doi.org/10.1016/j.molliq.2022.120239

This is a PDF file of an article that has undergone enhancements after acceptance, such as the addition of a cover page and metadata, and formatting for readability, but it is not yet the definitive version of record. This version will undergo additional copyediting, typesetting and review before it is published in its final form, but we are providing this version to give early visibility of the article. Please note that, during the production process, errors may be discovered which could affect the content, and all legal disclaimers that apply to the journal pertain.

© 2022 Published by Elsevier B.V.

Electric-field-induced patterns in a hockey-stick nematic

Jun Zhang,[1] Ying Xiang,[1*] Xiaoyu Ding,[1] Luguo Hao,[1]

[1]*School of Information Engineering, Guangdong University of Technology, Guangzhou 510006, People's Republic of China*

Supreet Kaur,[2] Golam Mohiuddin,[2#] Santanu Kumar Pal, [2*]

[2]*Department of Chemical Sciences, Indian Institute of Science Education and Research (IISER) Mohali, Sector-81, Knowledge City, Manauli 140306, India.*

Current Address: *Department of Chemistry, University of Science & Technology Meghalaya, Ri-Bhoi, Meghalaya-793101, India.*

Péter Salamon[3*],Nándor Éber,[3] Ágnes Buka [3]

[3]*Wigner Research Centre for Physics, Eötvös Lóránd Research Network, 1525 Budapest, P.O.Box 49, Hungary*

[*] Corresponding authors: frank_xiang68@qq.com; skpal@iisermohali.ac.in; salamon.peter@wigner.hu

Abstract

The response to applied electric field of a newly synthesized hockey-stick nematic 8-F-OH has been studied. Unusual pattern forming scenarios were found, which show rich variety as a function of frequency, temperature and initial director alignment. The behavior has been compared with those, observed in calamitic and bent-core nematics. Experiments show that contrary to calamitic nematics, here the elastically strongly deformed layers due to Fréedericksz transition play a decisive role in the formation of regular patterns. This is attributed to the cybotactic nematic phase with polar smectic clusters, where flexoelectricity might also have influence. Static and dynamic behaviors of the patterns have been characterized and an application idea is formulated.

Journal Pre-proofs

1. Introduction

Liquid crystals (LCs), being fluid and ordered medium, are a kind of functional materials with strong intrinsic anisotropy and sensitive response to external excitations. For example, nematic LCs (NLCs) exhibit remarkable electro-optic effects which are utilized in liquid crystal displays (LCDs) [1]. On the other hand, NLCs are a paradigm of complex, nonlinear systems which often respond by formation of patterns when driven out of equilibrium by external stimuli. A well-known manifestation of such pattern formation is electroconvection (EC) in NLCs, where a typically spatially periodic director deformation is accompanied by a material flow and space charge separation under the influence of an applied electric voltage [2].

NLCs may exhibit a large variety of EC patterns; the basic characteristics of these electric-field-induced patterns, such as the critical voltage (U_c), the onset wave vector ($\mathbf{q}$), and the frequency (f) and temperature (T) ranges of existence, are closely related to the electric transport properties of LCs and the boundary conditions [2, 3]. Thus investigation of EC phenomena and their underlying mechanisms have effectively contributed to the better understanding of the behavior and the physical properties of diverse NLCs as well as of some general features of other pattern forming systems (e.g. Rayleigh-Bénard convection in isotropic fluids, climatic phenomena). Besides, in view of the rich morphology of patterns, they offer valuable applications in the field of photonics [1]. Thus, exploration of patterns in LCs has been a hot topic for the past few decades.

Historically, EC phenomena have first been investigated in NLCs formed by rodlike (calamitic) molecules. The most encountered EC patterns occur in nematics with specific electric transport properties ($\Delta\varepsilon < 0$, $\Delta\sigma > 0$ or $\Delta\varepsilon > 0$, $\Delta\sigma < 0$; where $\Delta\varepsilon$ and $\Delta\sigma$ are the dielectric anisotropy and the conductivity anisotropy, respectively) and specific boundary conditions (planar or homeotropic), if the applied ac voltage exceeds a certain critical value U_c [2]. The pattern appears in a polarizing microscope as a sequence of stripes with alternating intensity or color, having a periodicity of $\Lambda \approx 2d$ (d is the thickness of the LC layer). The stripes run either perpendicular to the initial orientation $\mathbf{n}_0$ of planar samples (normal rolls (NR), $\mathbf{q} \parallel \mathbf{n}_0$) or in two degenerate, oblique directions (oblique rolls (OR), $\mathbf{q}$ and $\mathbf{n}_0$ making an acute angle

Journal Pre-proofs

$|\alpha| < 45°$). Their formation can be explained by the standard model of EC [4], a continuum description based on the feedback mechanism first recognized by Carr and Helfrich [5, 6]. At present, these patterns are known as "standard EC".

Later, EC patterns have also been found in NLCs with other combination of material properties ($\Delta\varepsilon > 0$, $\Delta\sigma > 0$ or $\Delta\varepsilon < 0$, $\Delta\sigma < 0$) [2], where EC should not occur according to the standard model. One representative of these "nonstandard EC" is the pattern composed of longitudinal stripes (LS), i.e., stripes running parallel or slightly oblique to $\mathbf{n}_0$ ($\mathbf{q} \perp \mathbf{n}_0$, or $|\alpha| > 45°$), which could be interpreted by inclusion of flexoelectricity into the standard model of EC, since an additional charge separation originating from the flexoelectric polarization of the periodically deformed state may also drive the convection [7].

Another pattern, which falls outside the frame of the standard model (and is thus counted as nonstandard EC) is the prewavy pattern [8]. It was observed in $\Delta\varepsilon < 0$ materials typically at higher frequencies than the patterns described so far (a few kHz and up) and is characterized with wide stripes (Λ being a multiple of $2d$) running normal to $\mathbf{n}_0$.

Besides rodlike molecules, some bent-core, banana-shaped ones might also form nematic (BCN) phase. They have attracted considerable interest, since their banana-shaped molecular structure might lead to peculiar physical properties [9, 10]. Especially, some BCNs have a tendency to form (anti)ferroelectric smectic clusters (cybotactic nematics) [11-14]. The presence of N_{cyb} phase was identified by the four-spot splitting of the diffuse small-angle X-ray scattering (SAXS) pattern [12]. Additionally, microrheological studies on the bent-core nematics are reported to be very useful in extracting information about underlying smectic clusters, where an approximate size of the clusters can be estimated using a simple model [14]. In some bent-core nematic systems, giant flexoelectric coefficients were reported, which were attributed not only to the molecular shape anisotropy [15-17], but additionally and perhaps more crucially, to the presence of reorientable short-range polar [18] or apolar [19] smectic clusters in the nematic phase. Reorientation of such clusters are expected to occur much slower than that of the nematic director due to the higher effective rotational viscosity of clusters; moreover, they may need larger reorienting torques. This explains why under certain conditions the larger contribution of clusters may be lost yielding regular (instead of giant) order of magnitude for the same

Journal Pre-proofs

molecules [20].

The cybotactic nature of BCNs may yield novel EC scenarios, like two kinds of PW patterns with diverging $U_c(f)$, the latter extending to unusually high f (up to MHz) and possessing $\frac{dU_c}{df} < 0$ [21, 22]. These compounds exhibited a sign inversion of $\Delta\sigma$ in the middle of the PW frequency range suggesting that the sign of $\Delta\sigma$ is irrelevant in the formation of the PW pattern. The occurrence of the PW patterns and their banana-specific behavior still awaits for theoretical explanation.

In the majority of BCNs reported so far, the two arms of the molecules are either identical or of similar length, resulting typically in a net molecular dipole moment nearly perpendicular to the long axis. Recently a special attention has been paid to strongly asymmetrical bent-core compounds, possessing two arms with substantially different lengths [23-25]. Resembling rather a hockey-stick, they represent an intermediate state in the molecular shape between rods and bananas. Hockey-stick materials have been reported to have a tendency to form a cybotactic nematic phase with polar smectic clusters. As a consequence, their behavior might differ from that of common NLCs, e.g., even though they do not seem to belong to ferroelectric nematics [26, 27], unusual polar switching could be detected in such materials [28-30].

Herein, we use pattern formation as a tool to explore the characteristics of a newly synthesized, polar hockey-stick compound 8-F-OH, in order to get deeper insight into the molecular self-assembly and the response to the external fields of this system. Our experimental results indicated that self-assembled EC rolls could be modified by properly adjusting the ac field, which provides a feasible way to tune the patterns for optical devices.

2. Materials and Methods

2.1. Materials

The experiments were performed on the asymmetrical bent-core (hockey-stick) compound 4-fluorophenyl (E)-3-((2-hydroxy-4-((4-(octyloxy)benzoyl)oxy) benzylidene)amino)-2-methylbenzoate (8-F-OH), whose molecular structure is presented in Figure 1. Synthesis and characterization of the compound by DSC, X-ray diffraction, dielectric spectroscopy and electro-optics is going to be published elsewhere [31]. According to quantum chemical calculations performed with the

Journal Pre-proofs

Gaussian 09 and GaussView 5.0 package and DFT calculations carried out to optimize the geometry of the compound using the B3LYP functional and the 6-311G (d, p) basis set, unlike symmetrical bananas, the dipole moment of 8-F-OH is nearly parallel to (making in statistical average an angle of about 27°) the long axis of the molecule (Figure1).

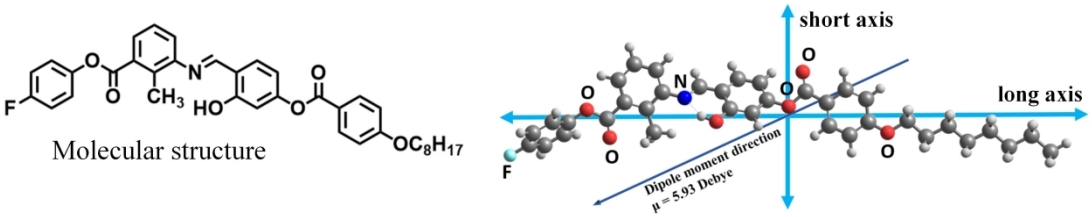

Figure 1. Molecular structure of the compound 8-F-OH

8-F-OH exhibits a cybotactic nematic mesophase (N_{cybC}) in a wide temperature range (> 80 ˚C) below the clearing point (T_c = 155.5 ˚C). The presence of cybotactic clustering in the nematic phase of compound 8-F-OH is proved with the help of homeotropic optical textures, temperature-dependent XRD studies, and dielectric spectroscopy [31] which are in accordance with the already reported results [13, 32-37].

Though compound 8-F-OH is not really a ferroelectric nematic, electro-optical studies indicated the presence of a ferroelectric-like switching and a spontaneous polarization in the order of 185 nC/cm^2, which are owing to the electric field-induced ordering of the cybotactic polar smectic clusters of the N_{cybC} phase [31]. By similar reasons, 8-F-OH is anticipated to possess flexoelectric coefficients enhanced compared to usual nematics.

Both planar and homeotropic cells could be prepared from 8-F-OH. For planar cells, polyimide (PI) Nissan SE150 was used, followed by antiparallel rubbing of the two substrates in order to obtain planar alignment along the direction $\mathbf{n}_0$, with 1-2 ° pretilt angle. For homeotropic cells, the two surfaces were treated by PI Nissan 7511L and then slightly rubbed along $\mathbf{n}_0$ to obtain a vertical alignment with broken azimuthal degeneracy, having an 88-89 ° pretilt angle. Both orientation techniques yielded uniform alignments. In the following measurements, cells with a thickness of d = 6 μm and an electrode area of 2.25 cm^2 were used. The initial director orientation of planar cells in the unperturbed state, $\mathbf{n_0}$, was chosen as the x-axis of our frame of

Journal Pre-proofs

reference.

2.2. Experimental setup for electro-optical measurements

The characteristics of patterns were probed by two, supplementary techniques: polarizing microscopy (POM) and laser diffraction. The morphologies of patterns could be captured by POM equipped with a fast CCD camera. In addition, as the periodic director distortions in the patterns form an optical grating, they diffract the incident linearly polarized He-Ne laser beam of polarization state $\mathbf{P}_{in}$ and wavelength $\lambda = 633$ nm. In the diffraction setup (Figure 2), the temporal evolution as well as the polarization state of the diffraction fringes could be detected by a fast photodetector (DET36A/M from Thorlabs) and a polarimeter (PAX1000VIS from Thorlabs), respectively.

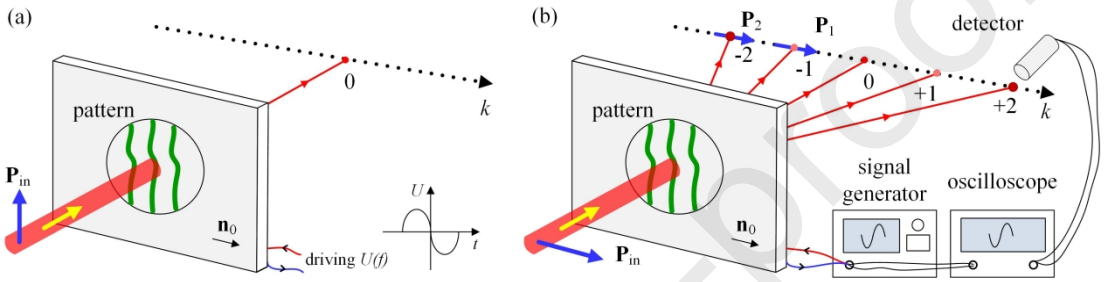

Figure 2. Geometry of the diffraction setup. (a) With $\mathbf{P}_{in} \perp \mathbf{n}_0$, no diffraction was observed; (b) with $\mathbf{P}_{in} \parallel \mathbf{n}_0$, diffraction fringes of various order k (0, ± 1, ± 2, …) with corresponding polarization states ($\mathbf{P}_0$, $\mathbf{P}_1$, $\mathbf{P}_2$, …) appear.

The sample temperature was kept by a heating stage (Linkam LTS420) driven by a temperature controller (TMS 94). In addition, a sinusoidal ac voltage of rms value U with different frequency f was applied to the samples through an amplifier; the resulting electric field $\mathbf{E}$ was perpendicular to the cell substrates (z-axis). The measurements presented below were performed in the temperature range of 70–155 ˚C, in the N_{cybC} phase.

2.3. Permittivity and conductivity measurement

Usually, anisotropies of the dielectric permittivity $\Delta\varepsilon$ and that of the electrical conductivity $\Delta\sigma$ are key factors governing the formation and behavior of EC patterns.

Journal Pre-proofs

By using the IM3536 precision impedance analyzer (f range of 4 Hz – 4 MHz), the temperature and frequency dependences of the permittivity ($\varepsilon_{\parallel}$ and $\varepsilon_{\perp}$) and conductivity ($\sigma_{\parallel}$ and $\sigma_{\perp}$) of 8-F-OH could be determined; $\varepsilon_{\parallel}(T)$ and $\varepsilon_{\perp}(T)$ are plotted in Figure 3 for some selected frequencies.

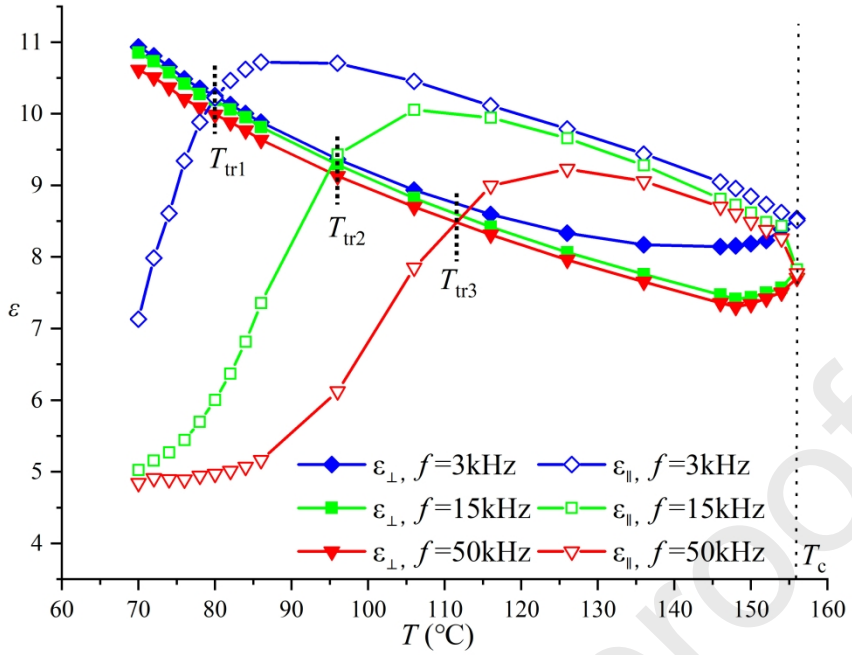

Figure 3. The effect of temperature on the anisotropic dielectric parameters at representative frequencies. At the sign inversion temperature $T_{tr}(f)$, $\varepsilon_{\parallel} = \varepsilon_{\perp}$.

Thorough inspection of the results indicates that at low frequencies ($f \leq 2$ kHz), $\Delta\varepsilon > 0$ fulfils for the whole nematic phase; whereas at higher frequencies ($f \geq 2$ kHz) there is a sign inversion temperature T_{tr}; $\Delta\varepsilon > 0$ holds only when $T > T_{tr}$, while for $T < T_{tr}$ one finds $\Delta\varepsilon < 0$. The reason for the sign change is a relatively low frequency dielectric dispersion of $\varepsilon_{\parallel}$, which shifts to higher frequency with temperature. Consequently, when f increases, T_{tr} shifts to higher temperatures accordingly. Experiments show that, as expected, the sign of $\Delta\varepsilon$ plays a decisive role in producing Fréedericksz transition (FT) and EC patterns.

As for the conductivity anisotropy, though $\Delta\sigma(f, T)$ depended on f and T, its positive sign ($\Delta\sigma > 0$) persisted for the frequencies shown, almost over the entire nematic temperature range, except at very low T.

3. Experimental results

Journal Pre-proofs

It was observed that depending on T and f, various patterns appeared, whose critical voltage U_c as well as the onset morphologies (especially, the direction and the magnitude of the wave vector **q**) differed significantly from each other. Observations indicated that studying the pattern formation should focus onto two distinct frequency ranges, because the substance experiences an unusually low-frequency dielectric dispersion of $\varepsilon_{\parallel}$. That leads to change of sign of $\Delta\varepsilon$ (see Figure 3), which is a decisive quantity in the behavior in electric field. When driven by an ac voltage of low frequency (20–200 Hz), where $\Delta\varepsilon$ is positive, the first instability is the homogeneous Fréedericksz transition. On that elastically deformed state, stripe patterns arise at any temperature. In view of the direction of **q,** the nematic temperature range could be divided into three sections. At low temperatures longitudinal stripes (LS, $\mathbf{q} \perp \mathbf{n}_0$), at high temperatures normal stripes (NS, $\mathbf{q} \parallel \mathbf{n}_0$), while at intermediate temperatures oblique stripes (OS) occurred. In contrast to these, if the frequency was increased up to high values (3–50 kHz), normal stripes of larger wavelength, a kind of prewavy (PW) pattern appeared instead; its frequency range of existence, however, depended strongly on the sample temperature.

In the following, we report on detailed characterization of the above patterns by varying the temperature, frequency, and voltage, exploring the correlation between patterns and FT occurring in this nematic compound. The static and dynamic characteristics of patterns were examined by POM and diffraction technique, respectively. We should remind here that while the occurrence of FT is governed solely by the sign of $\Delta\varepsilon$ and the cell configuration, in the formation of patterns both $\Delta\varepsilon$ and $\Delta\sigma$ are involved.

3.1. POM observations:

3.1.1 Patterns at low frequency driving

Let us recall that in the low-frequency range of several tens Hz (20 Hz < f < 200 Hz), $\Delta\varepsilon > 0$ and $\Delta\sigma > 0$ fulfils in the whole nematic temperature range. Under these conditions the EC patterns occurring in the system should be characterized as nonstandard EC.

In a planar cell at $U = 0$, an unperturbed initial state with uniform and pattern-free texture is observed, as shown in Figure 4(a). Due to the positive dielectric anisotropy, FT occurred first when U increased over a threshold U_F ($U \geq U_F$). FT manifested itself

Journal Pre-proofs

as two, spatially distributed domains, where the color in each domain was uniform, but differed from each other, as shown in Figures 4(b) and 4(c). With increasing U, the color inside each domain altered but still remained uniform, and the shape of the wall separating the two domains also changed; this revealed that after FT two kinds of director deformations are present in the sample.

3.1.1.1 Normal stripes

Increasing the voltage well above U_F in the high temperature range (T_{r2} = 122 °C < T < T_c = 155.5 °C), first the texture of the sample turned into a uniform dark state with crossed polarizers (Figure 4(d)), indicating that the director mostly reoriented perpendicular to the cell surface, yielding a quasi-homeotropic state. Afterwards, if we continued increasing U above another critical voltage U_c ($U > U_c >> U_F$), pattern NS with undulated, thin and dim stripes running perpendicular to $\mathbf{n}_0$ appeared, whose periodicity Λ was approximately the cell thickness d.

In order to check the underlying director distribution of the pattern, shadowgraph images were also captured, where the analyzer (**A**) was removed and the orientation of the remaining polarizer (**P**) was changed with respect to $\mathbf{n}_0$, into the angles of 0°, 45° and 90°, as shown in Figures 4(e), 4(f), and 4(g), respectively. Unsurprisingly, the contrast of the NS pattern is maximal at extraordinary illumination ($\mathbf{P} \parallel \mathbf{n}_0$), while NS becomes invisible at ordinary illumination ($\mathbf{P} \perp \mathbf{n}_0$). This indicates that the director deformation occurs in the x-z plane.

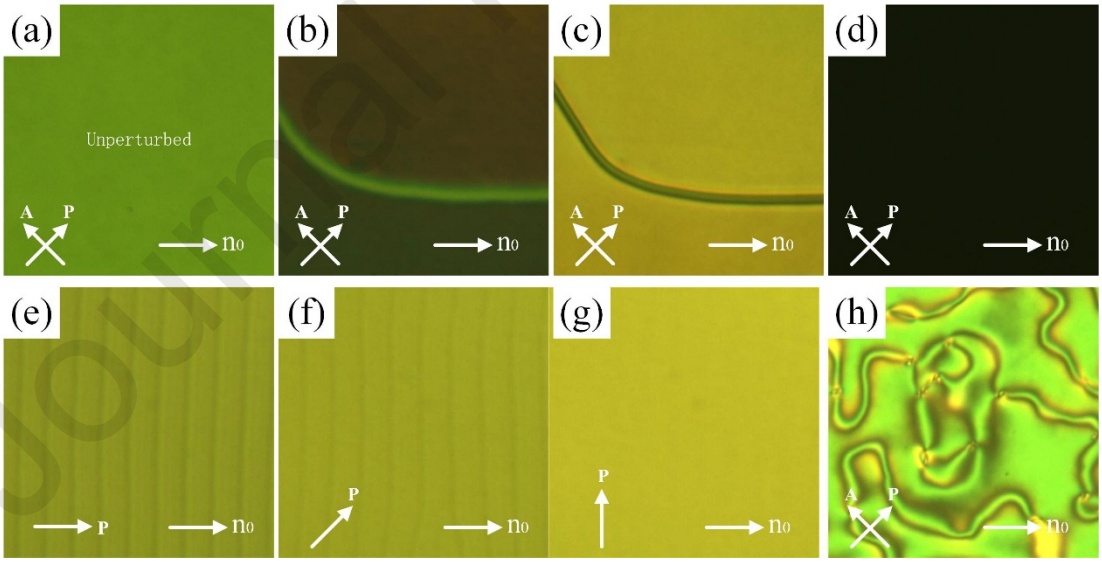

Figure 4. In planar cell, at the high temperature of T = 152 °C, driven by ac field with

f=100 Hz, FT deformation and normal pattern appears in turn as U increases. (a) texture of the unperturbed state at U = 0 V; (b) FT deformation with two coexisting domains, after applying threshold voltage U_F = 9.0 V for 10 s; (c) FT deformation at U = 11.0 V; (d) uniform dark state with U = 12.5 V; (e)–(g) emergence of normal pattern with $\Lambda \cong$ 12.5 μm, at critical U_c = 13 V, at different orientations of a single polarizer; (h) after cancelling U, the sample could not restore the initial unperturbed state. The size of snapshots is 100*100 μm; **P**, **A** and $\mathbf{n}_0$ denote the polarizer, the analyzer and the surface alignment.

It should be stressed that $U_c > U_F$ implies that the formation of FT is a precondition for producing NS; i.e., NS cannot occur directly by skipping FT. Consequently, a transformation between the FT state and the patterned state takes place upon increasing U. In order to track this transformation, U was increased slowly in small (0.1 V) steps, allotting enough time (~10 s) after each voltage change for system stabilization; the corresponding morphological changes are demonstrated by the sequences of snapshots in Figure 5. At the beginning, FT was present with two coexisting domains as shown in Figure 5(a) (like in Figures 4(b) and 4(c)); here the orthogonal polarizers were replaced by parallel ones in order to observe the texture clearly. Increasing U to a critical voltage U_{c1} = 12.4 V, NS started to grow in one domain, whereas the other domain still stayed in the FT state (Figure 5(b)). Further increasing U to another critical voltage U_{c2} = 14.6 V, both domains were occupied by NS (Figure 5(c)). Finally, at much higher U (U = 18.8 V), the system turned into a chaotic state (Figure 5(d)). The small asymmetry in the pattern onset of the two domains can be attributed to differences in the director distortion and surface anchoring between them.

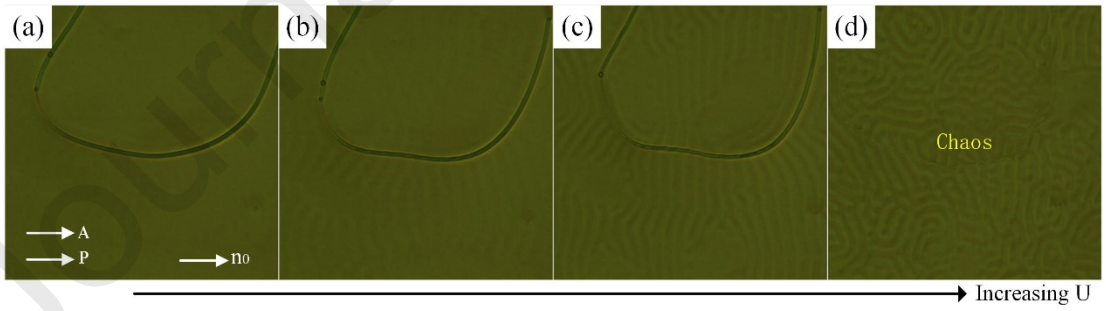

Figure 5. In planar cell, at the high temperature of T = 152 °C, driven by ac field with f=100 Hz, as U gradually increases, the system undergoes a transformation from FT

to normal pattern. (a) The FT state with two domains at $U = 11.5$ V; (b) normal pattern present in one domain only at $U_{c1} = 12.4$ V, while the other domain remained in the FT state; (c) at $U_{c2} = 14.6$ V both domains are occupied by normal pattern; (d) chaotic state at $U = 18.8$ V. (The size of snapshots is 200*200μm)

Besides determining the above static morphologies of patterns, temporal evolution of the pattern buildup and decay upon switching the driving ac voltage on and off were also recorded via time sequences of snapshots, as illustrated in Figure 6. It can be seen that when the ac voltage $U = 1.15\ U_c$ was switched on, FT emerged first, followed by the appearance of NS pattern in one FT domain; subsequently NS formed in another FT domain too. After cancellation of the ac field, the pattern decayed immediately; then the FT state relaxed slowly back to the initial unperturbed state. Observations concluded that the buildup process of NS is slower, while its decay process is faster compared to those of FT.

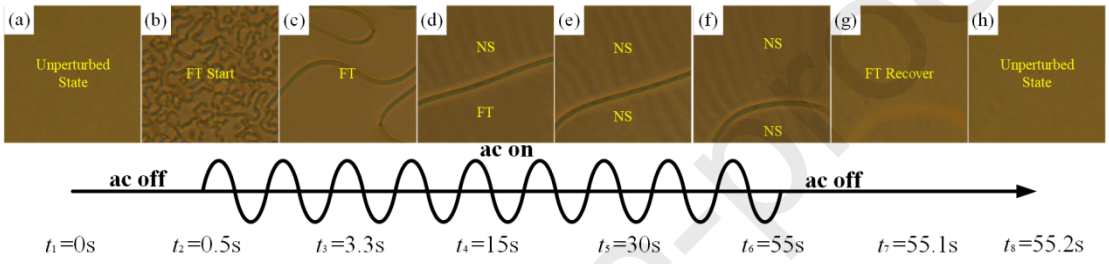

Figure 6. Time evolution of FT and the subsequent NS pattern at $T = 152$ °C, upon the switching on/off the ac field at $U = 1.15\ U_c$ and $f = 100$ Hz. (a)(h) the unperturbed state; (b)(c) emergence and growth of the FT state; (d)(e) appearance of NS one by one in different FT domains; (g) relaxation to the FT state. (size 100 * 100 μm)

We note here that if the voltage is switched off in the chaotic state (i.e. at $U >> U_c$), the system does not relax directly to the initial, unperturbed state; instead, an irregular set of disclination lines, a kind of Schlieren texture forms, making the texture non-uniform (Figure 4(h)). Recovering the uniform, unperturbed state under isothermal conditions may need a very long time; alternatively, the sample may be heated into the isotropic phase and then cooled back into the nematic phase.

The behavior of homeotropic samples have also been tested. In contrast to planar ones, in homeotropic cells, neither FT no pattern formation was detected, no matter how high U was applied. Instead, only a uniform dark state (corresponding to light

Journal Pre-proofs

extinction) was present at crossed polarizer and analyzer. This is a really new feature of the system. In calamitic nematics, if roll patterns arise in the quasi-homeotropic, Fréedericksz distorted state, they appear in the initially homeotropic sample as well. In contrary here, the prerequisite for the patterns are the elastically deformed layers close to the substrate surfaces.

3.1.1.2 Longitudinal stripes

When T is in the low temperature range of $T < T_{r1} = 87$ °C, in a planar cell, the situation is similar to the one reported above, except that the NS pattern was replaced by longitudinal stripes (LS). Namely, from the unperturbed state (Figure 7(a)) FT appeared first at U_F (Figure 7(b) and 7(c)), which was then followed by the emergence of the LS pattern (Figure 7(d)), if U increased further above the critical voltage U_c. The LS pattern manifested itself as thick and sharp stripes parallel to $\mathbf{n}_0$, with the periodicity Λ about the order of the cell thickness d. As U_c is just a little higher than U_F, the pattern began to grow before the LC director reoriented perpendicularly. Consequently, the uniform tilted orientation is the ground state for producing the LS pattern.

In order to examine the optical properties of the LS, again the shadowgraph technique was used to check, how the contrast varies depending on the direction of the polarizer, as shown in Figures 7(e)–7(g). The strongest contrast was obtained at $\mathbf{P} \parallel \mathbf{n}_0$ (Figure 7(e)), whereas the lowest occurred at $\mathbf{P} \perp \mathbf{n}_0$ with hardly, but still visible stripes (Figure 7(g)). These characteristics suggest that LS might involve some twist deformation (i.e. azimuthal modulation in the cell plane).

When U was cancelled after the occurrence of the LS pattern, the system relaxed to the initially unperturbed state with uniform texture (Figure 7(h)).

Journal Pre-proofs

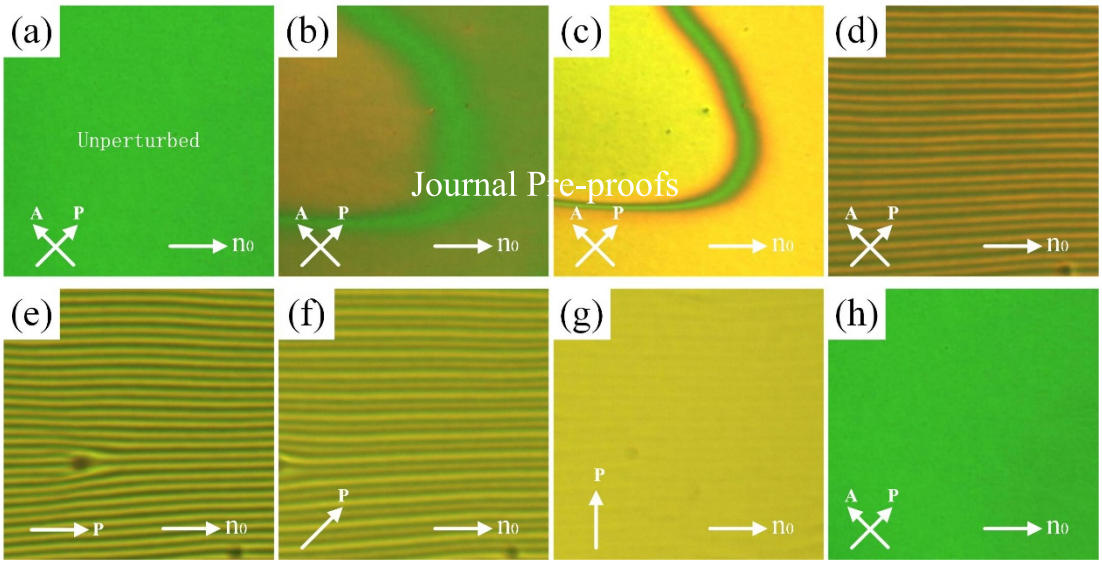

Journal Pre-proofs

Figure 7. In planar cell, at low temperature of $T = 81$ °C, driven by ac field with $f =$ 50 Hz and increasing U, FT deformation and longitudinal pattern occurred successively. (a) Texture of the uniform unperturbed state at $U = 0$ V; (b) FT deformation with two coexisting domains, after applying threshold voltage $U_F = 6.5$ V for 10s; (c) FT deformed state at $U = 7.0$ V; (d) emergence of longitudinal pattern at the critical voltage $U_c = 10$ V, with $\Lambda \cong 7.5$ μm; (e)(f)(g) longitudinal pattern observed with only one polarizer of different orientation, at $U = 16$ V; (h) after cancelling U, the sample restores the initial unperturbed state. The size of snapshots is 100*100μm; **P**, **A** and $\mathbf{n}_0$ denote the polarizer, analyser and surface alignment, respectively.

Similarly to the case of NS, the transformation from FT to LS upon increasing U is illustrated by sequences of snapshots in Figure 8. As U grows, FT appears first in the form of two domains (Figure 8(a)); then LS emerges in one domain, whereas the other domain still stays in the FT state (Figure 8(b)). Next, LS appears in another FT domain too (Figure 8(c)); finally, the system turns into a chaotic state at high enough U (Figure 8(d)).

Journal Pre-proofs

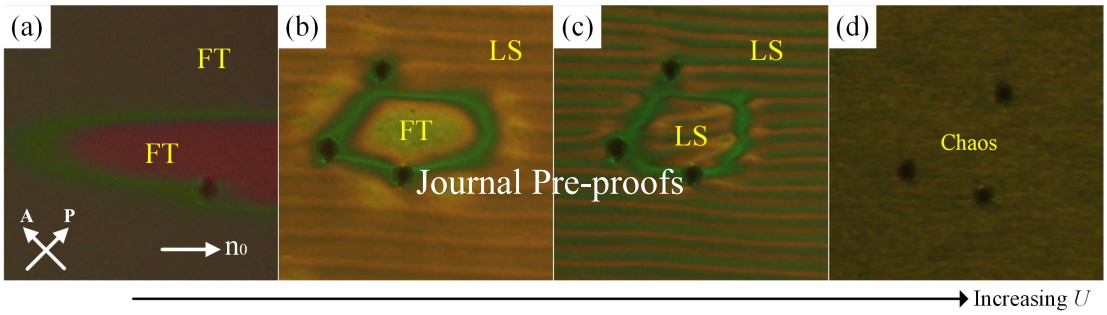

Journal Pre-proofs

Figure 8. Transformation between FT and longitudinal pattern upon gradual increase of U, illustrated by a sequence of microphotographs at T = 81 °C and f = 50 Hz. (a) FT state exhibiting two domains at U = 9.0 V; (b) longitudinal pattern present in one domain at U_{c1}= 10.2 V, while the other domain remains in the FT state; (c) both domains are occupied by longitudinal pattern at U_{c2} = 12.0 V; (d) chaos at U= 43 V. (size 100*100μm)

In addition to the static behavior, the temporal evolution on a large time scale, i.e. the response of LS pattern to switching the ac-field on and off, was monitored by taking a sequence of POM snapshots, as shown in Figure 9. Similarly to NS, the buildup and decay processes of LS involve the FT effect. The formation of LS was much slower, and the relaxation of LS was much faster than that of the FT.

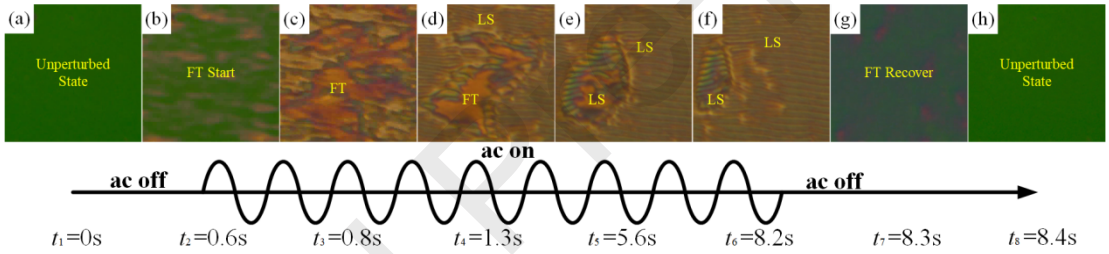

Figure 9. Time evolution of FT and the subsequent longitudinal pattern during switching on and off the ac field at T = 81 °C, U = 1.15 U_c and f = 50 Hz. (a)(h) the unperturbed state; (b)(c) emergence and growth of the FT state; (d)(e) appearance of LS one by one in the different FT domains; (f) stable LS pattern; (g) relaxation of the FT state. (size 100*100μm)

Besides the onset morphology, the critical voltage U_c is also a key parameter characterizing the pattern behavior, which strongly depends on f and T, as shown in Figure 10. Special attention was paid to the critical behavior of $U_c(T)$, which might give some clue about the origin of the pattern forming phenomenon. For NS, as the

increasing T approaches T_c, U_c held steady; however, for LS, as T decreases toward crystallization, U_c grew significantly and even diverged. The latter may be attributed to strong variation of the material parameters, which may be the consequence of the increasing size and role of the cybotactic clusters.

In contrast to planar ones, for the homeotropic cell, neither FT nor patterns were present, irrespective of how high the U was.

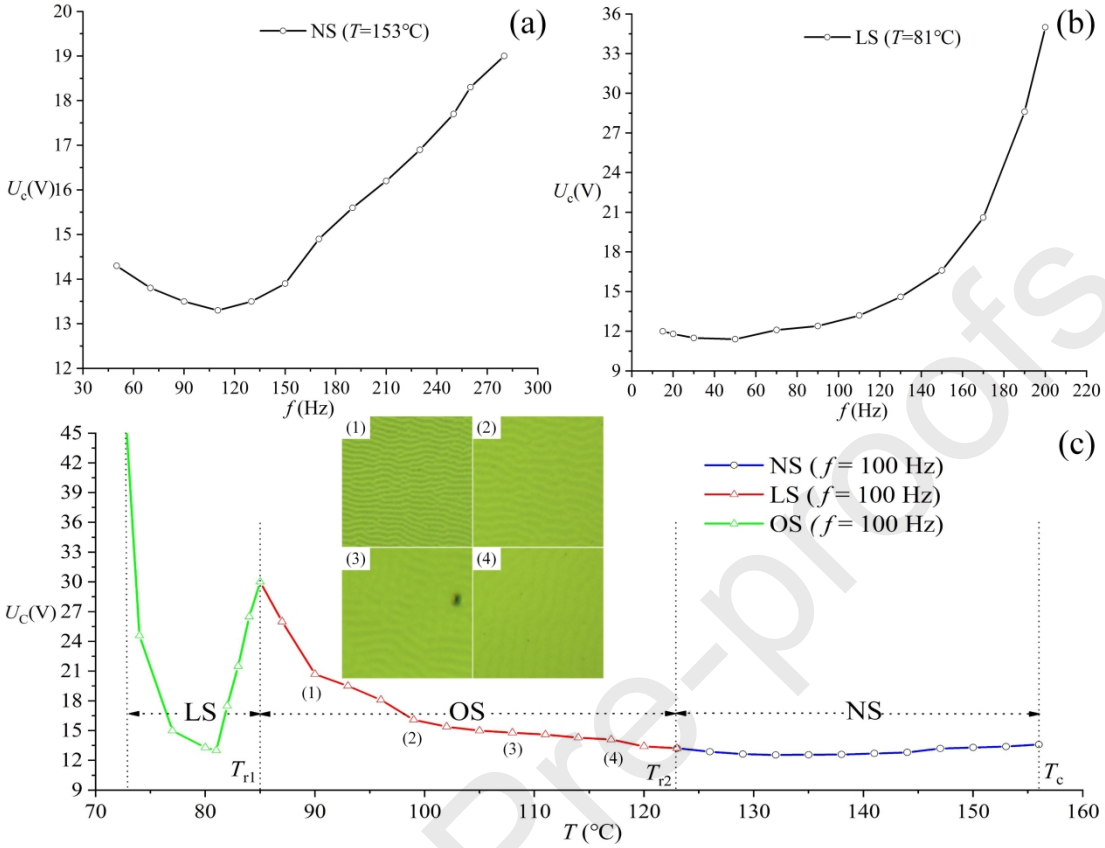

Figure 10. Dependences of the critical voltage U_c(f, T) on temperature and frequency. (a)(b) U_c (f) of NS and LS, respectively, at a fixed T, (c) U_c(T) of NS, LS and OS at fixed f, as well as snapshots of the OS pattern at the temperatures (1)–(4).

3.1.1.3 Oblique stripes

If T is in the intermediate temperature range of T_{r1} = 87 °C < T < T_{r2} = 122 °C, the sample still undergoes FT first upon enhancing U, but later, instead of a regular pattern associated with a single **q**, an irregular zigzag pattern could be observed. In this pattern, the stripes are oblique (OS) and can be characterized by two degenerate wave vectors $\mathbf{q}^+$ and $\mathbf{q}^-$, which enclose angles $\pm\alpha$ with $\mathbf{n}_0$ (see the snapshots in Figure 10(c)). The angle α as well as U_c of this pattern, strongly depend on the temperature T,

Journal Pre-proofs

as shown in Figure 10(c). When T increased approaching the high temperature range ($T \rightarrow T_{r2}$), the stripes tended to align perpendicularly ($\alpha \rightarrow 0°$), resembling NS; whereas when T decreased approaching the low temperature range ($T \rightarrow T_{r1}$), the stripes preferred to orient longitudinally ($\alpha \rightarrow 90°$), like in LS. Thus it can be concluded that OS is an intermediate state representing a gradual transformation between the NS and LS patterns.

It can be deduced from Figure 10(c), that $U_c(T)$ of OS and NS are smoothly connected at $T = T_{r2}$. Surprisingly, however, $U_c(T)$ exhibits a cusp at $T = T_{r1}$ at the transition from LS to OS; though there is no U_c gap between the adjacent patterns. As no underlying structural transition has been detected at this temperature, finding the origin of the cusp requires further investigations.

3.1.2 High frequency patterns

While low frequency patterns could be observed in the entire N_{cybC} temperature range of 8-F-OH, this does not hold for high frequencies. If f increased up to several or even tens of kHz, a prewavy (PW) pattern could be detected, emerging directly from the homogeneous, planar state at $U > U_c$, but only within a specific temperature range (T_{d1} = 81 °C ≤ T ≤ T_{d2} = 111 °C). More precisely, these patterns existed at a certain combination of frequencies and temperatures, as shown by the cyan region in Figure 11(a). In this f-range the dielectric anisotropy is negative, thus one does not expect a Fréedericksz transition in a planar cell.

The PW pattern manifested itself as strong and broad stripes perpendicular to $\mathbf{n}_0$, with a periodicity Λ being a multiple of the thickness d. After withdrawing U, PW quickly decayed and the system relaxed to the initial unperturbed state with uniform texture.

Besides the range of existence of PW (Figure 11(a)), the corresponding U_c depends strongly both on f and T **(**Figure 11(b)**)**. It was also observed that the periodicity Λ shortened with increasing f, as shown in Figure 12. The same Λ shortening can be seen also upon increasing U (Figure 13), however, it is accompanied by the appearance of long defects in the structure (Figures 13(c)-13(d)).

In the homeotropic cell, Fréedericksz transition occurred within the f and T ranges producing PW in planar cell. Afterward, even increasing U to very high values, no patterns were observed. The presence of FT with the absence of patterns reiterates that FT is not the precondition for PW, in contrast to that for NS or LS. This again points

Journal Pre-proofs

to a difference in the behavior of 8-F-OH compared to calamitic nematics, since e.g. in n-(4-methoxybenzylidene)-4-butylaniline (MBBA) the PW pattern may be seen in homeotropic cells too [8].

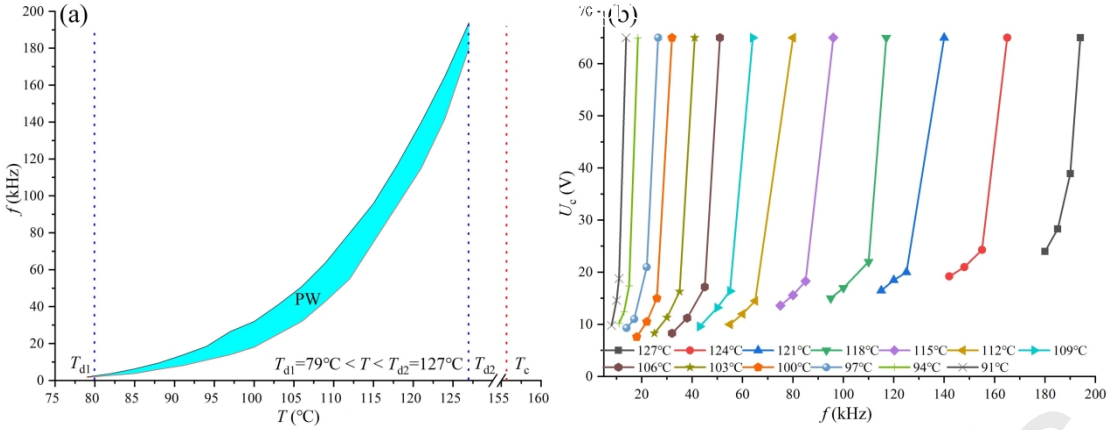

Figure 11. (a) Pattern PW exists in the cyan-marked frequency and temperature ranges; (b) dependences of U_c on f and T.

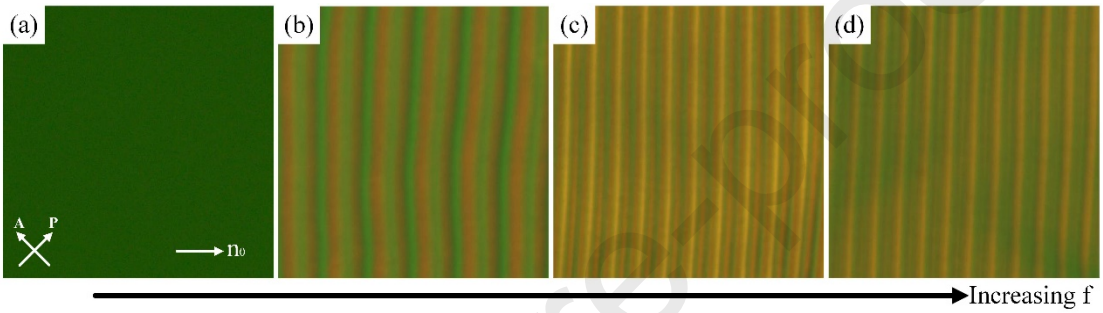

Figure 12. Morphological changes of PW at U_c at different f in a planar cell, at T = 94 °C, (a) The unperturbed state; (b) $\Lambda \approx 17.8$ μm, U_c = 35 V and f = 15 kHz; (c) $\Lambda \approx 9.8$ μm, U_c = 57 V and f = 19 kHz; (d) $\Lambda \approx 9.0$ μm, U_c = 63 V and f = 20 kHz. (The size of snapshots is 100*100μm)

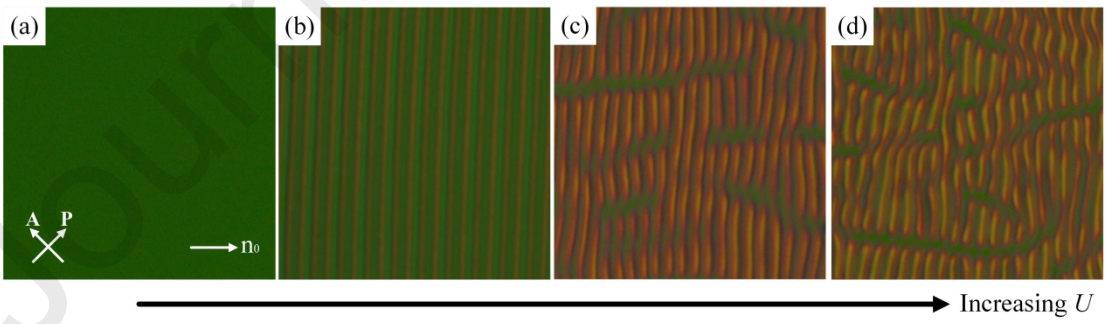

Figure 13. Representative snapshots of the PW pattern in a planar cell at T = 94°C

Journal Pre-proofs

and f = 17 kHz, upon increasing U above U_c (f = 17 kHz). (a) The unperturbed state; (b) $\Lambda \approx$ 9.8 μm, U = 56 V; (c) $\Lambda \approx$ 9.4 μm, U = 67 V; (d) $\Lambda \approx$ 9.1 μm, U = 69 V. (The size of snapshots is 100*100μm)

3.1.3 Polarity dependent U_c of patterns

There are indications [31] that 8-F-OH exhibits a kind of polar nature, thus the question arises whether this behavior (the occurrence of a spontaneous polarization $\mathbf{P}_s$) has an influence on pattern formation, or has not. In order to obtain information on that, LS and PW were studied under stimuli of superposed ac and dc voltages too. The driving waveforms and the onset morphologies as well as U_c of these patterns are shown in Figure 14. It was observed that for LS, produced at the low frequency of f = 50 Hz, the critical voltages for positive and negative unipolar driving (Figures 14(a) and 14(c), respectively) are equal, and higher than that at bipolar driving (Figure 14(b)) ($U_c^+ = U_c^- > U_c^\pm$), whereas the corresponding morphologies were almost the same. In contrast, at the high frequency of f = 30 kHz, PW has $U_c^+ = U_c^- \approx U_c^\pm$ with the same onset morphologies.

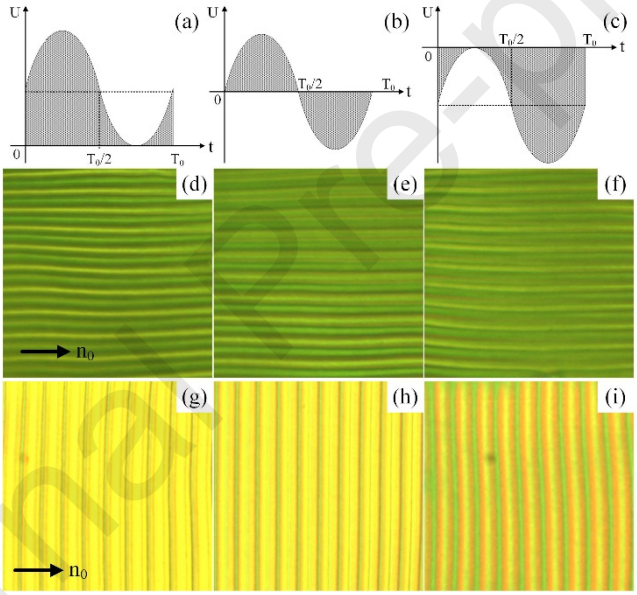

Figure 14. (a)(b)(c) Waveforms of the positive unipolar, bipolar and negative unipolar driving fields, respectively; (d)(e)(f) onset morphologies of LS, subjected to waveforms in (a)(b)(c), at T = 81 °C and f = 50 Hz , with $U_c^+ = 31\ V$, $U_c^\pm = 29.5\ V$ and $U_c^- = 31\ V$, respectively; (g)(h)(i) onset morphologies of PW, subjected to waveforms in (a)(b)(c), at T = 104 °C and f = 30 kHz , with $U_c^+ = 28\ V$, $U_c^\pm = 28\ V$

Journal Pre-proofs

and $U_c^- = 28\,V$, respectively. (The size of snapshots is 100*100μm; and U is the peak-to-peak value here)

Independence of the threshold voltage of PW on the dc offset is not surprising, as at such high f, $\mathbf{P}_s$ is not expected to play any role. Nevertheless, it has yet to be confirmed whether the threshold voltage increment of LS found at low f at unipolar driving is related to the polar behavior (the occurrence of a $\mathbf{P}_s$) or is the result of other (e.g. conductivity related) effects. We note here that recent studies on standard EC of calamitic nematics at combined (ac + dc) driving pointed out that adding a dc voltage may lead to unexpected increase of U_c, including a suppression of pattern formation [38, 39], due to dc-voltage-induced reduction of the conductivity and its anisotropy.

3.2. Diffraction observations

Besides recording the POM images of the patterns, diffraction of a linearly polarized laser beam was also applied in order to gather complementary information about the polarization states and the dynamics of the observed structures.

3.2.1 Diffraction fringes and their polarization states

First, in order to explore the anisotropic features of the diffraction, we studied the polarization state of the fringes when changing the angle between the polarization of the incident laser beam $\mathbf{P}_{in}$ and $\mathbf{n}_0$, which gives information about the director distribution in the patterned state, as shown in Figures 15, 16 and 17.

It was observed that NS (Figure 15), and PW (Figure 17) show similar behavior: only the configuration $\mathbf{P}_{in} \parallel \mathbf{n}_0$ gives rise to strong diffraction fringes, whereas diffraction disappears at $\mathbf{P}_{in} \perp \mathbf{n}_0$. Furthermore, the polarization states $\mathbf{P}_1$ and $\mathbf{P}_2$ of the 1st and 2nd order fringes, respectively, were also determined: both being linearly polarized and parallel to $\mathbf{n}_0$ ($\mathbf{P}_1 \parallel \mathbf{n}_0$ and $\mathbf{P}_2 \parallel \mathbf{n}_0$). This indicates that the director remains in the x-z plane, performing only splay-bend deformation without twist.

In contrast, diffraction occurs at both $\mathbf{P}_{in} \parallel \mathbf{n}_0$ and $\mathbf{P}_{in} \perp \mathbf{n}_0$ for LS (Figure 16). While at $\mathbf{P}_{in} \parallel \mathbf{n}_0$, $\mathbf{P}_1$ and $\mathbf{P}_2$ of the 1st and 2nd order fringes, respectively, are both linearly polarized and parallel with $\mathbf{P}_{in}$; $\mathbf{P}_1$ of the 1st order fringe is linearly polarized, but perpendicular to $\mathbf{P}_{in}$ at $\mathbf{P}_{in} \perp \mathbf{n}_0$. This is a sign that the director distribution involves twist deformation.

As a summary we can conclude that the polarization direction of the diffracted

Journal Pre-proofs

light always coincided with that of the incident one, independent of the order or of the pattern type.

The power distribution between the diffraction fringes of various orders were also detected for the patterns:

① for NS, the intensity of the 1st order fringe is much stronger than that of the 2nd order one;

② for LS, at $\mathbf{P_{in}} \parallel \mathbf{n_0}$, the intensity of the 2nd order fringe is moderately stronger than that of the 1st order one, which still is visible; at $\mathbf{P_{in}} \perp \mathbf{n_0}$, only the 1st order fringe is observable, whereas the 2nd order fringe disappeared;

③ for PW, the intensity of the 2nd order fringe is far stronger than that of the 1st order one, while the 1st order fringe almost vanishes.

We note here that knowing the director distribution within the pattern, the characteristics of the diffracted light (the polarization direction and the intensity of the various orders) could be calculated as described in a recent theoretical paper [40]. Unfortunately, the driving mechanism and thus director distribution of the nonstandard EC patterns studied above still awaits exploration, hence the comparison of diffraction experiments with the theory could not yet been performed.

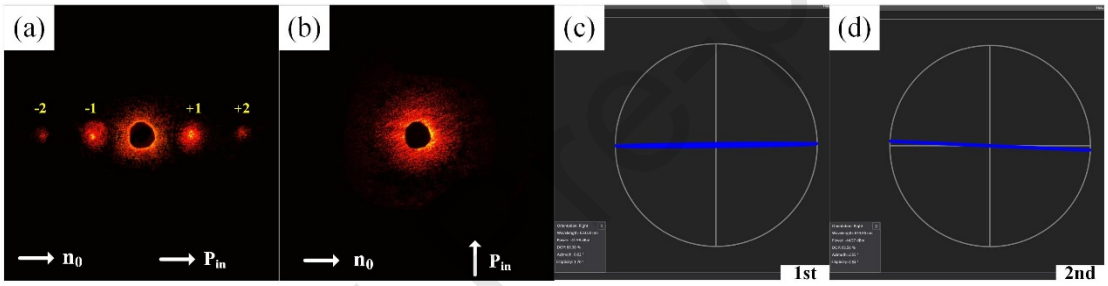

Figure 15. Diffractions occurring on NS at $T = 152$ °C, $f = 100$ Hz and $U = 11$ V. (a) Diffraction fringes at $\mathbf{P_{in}} \parallel \mathbf{n_0}$; (b) diffraction fringes at $\mathbf{P_{in}} \perp \mathbf{n_0}$; (c)(d) polarization directions (blue lines) of the 1st and 2nd order diffraction spots in (a), respectively.

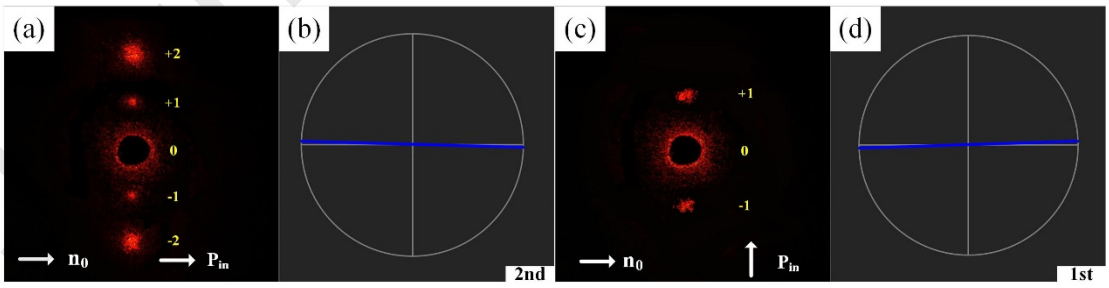

Figure 16. Diffraction on LS at $T = 81$ °C, $f = 50$ Hz and $U = 14.5$ V. (a)(c)

diffraction fringes at $\mathbf{P_{in}} \parallel \mathbf{n_0}$ and $\mathbf{P_{in}} \perp \mathbf{n_0}$, respectively; (b)(d) polarization directions of the 2nd and 1st order diffraction spots in (a) and (c), respectively.

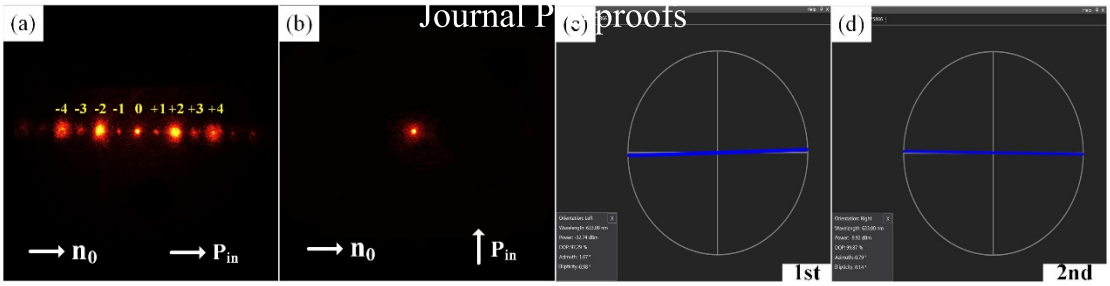

Figure 17. Diffraction induced by PW at $T = 94$ °C, $f = 17$ kHz and $U = 39$ V. (a) Diffraction fringes at $\mathbf{P_{in}} \parallel \mathbf{n_0}$; (b) diffraction fringes at $\mathbf{P_{in}} \perp \mathbf{n_0}$; (c)(d) polarization directions of the 1st and 2nd order diffraction spots in (a), respectively.

3.2.2 Time evolution of the buildup and decay processes of patterns

The time evolution of patterns was characterized by monitoring the changes in the diffraction efficiency η; here η_1 and η_2 are defined as the ratio of the intensity of the 1st and 2nd order diffraction spots, respectively, to the intensity of the incident probe beam. It can be easily identified in Figure 18 that NS, PW and LS yield weak, moderate and strong efficiency, respectively.

It was observed that for all patterns at U being just slightly above U_c, the characteristic time of the buildup process was much longer than that of the decay process. Namely, while it took about several seconds to form patterns, the decay time upon turning U off was less than 0.2 second, as seen in Figure 18. However, by enhancing U, the buildup process could be accelerated significantly, whereas the decay process was almost unaltered. This observation is in agreement with previous findings [41]. The decay time is only independent of the driving voltage when the wavenumber is zero, e.g. in case of the homogeneous Fréedericksz transition. For a patterned mode the reciprocal value of the decay time is proportional to the square of the wavenumber [42, 43].

It should be noted that the buildup processes of NS and LS resulted in a strong and sharp scattering peak, whereas no such peak occurred for PW. A careful inspection indicated that this peak is induced by the transition from FT to NS or LS, which is absent in PW.

Journal Pre-proofs

We note here that though not directly seen in the diffraction, adjustment of the pattern wave vector upon changes of the driving voltage or its frequency occurs via creation, motion and annihilation of defects in the EC pattern [44, 45]. These defects thus crucially affect the transition times. Recent studies also pointed out that interaction of EC with topological defects may yield new dynamic features [46-48].

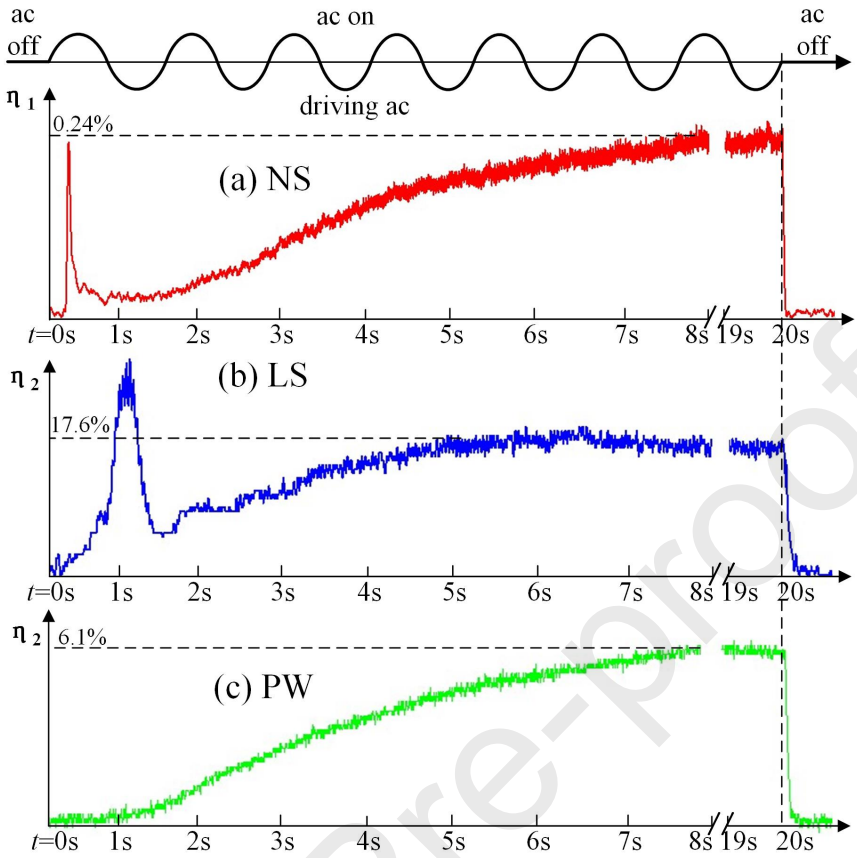

Figure 18. Temporal evolution of the buildup and decay processes of the patterns upon switching the ac field on and off at $U = 1.15\ U_c$. (a) NS, with $t_{buildup}$ = 6.5 s and t_{decay} = 48 ms, at f = 100 Hz and T = 152 °C; (b) LS with $t_{buildup}$ = 5.0 s and t_{decay} = 170 ms, at f = 50 Hz and T = 81 °C; (d) PW with $t_{buildup}$ = 8.0 s and t_{decay} = 130 ms, at f = 20 kHz and T = 96 °C.

3.2.3 Dynamics of patterns within a single cycle of the driving ac voltage

Dynamics of patterns on a short time scale, in response to the oscillation of the driving ac voltage within a single period t_0, provides another viewpoint to explore the underlying mechanism of pattern formation. Indeed, Figures 19(a)—(c) demonstrate different time characteristics for NS, LS and PW, respectively. It was observed that when f is rather high (f = 17 kHz), the diffraction intensity of PW remains constant

Journal Pre-proofs

with time, revealing that the director is stationary. However, if f is low (f = 50 Hz), the diffraction intensities of NS and LS oscillate strongly with a frequency of 2f, demonstrating that the directors are stationary only in the leading order, with the 2f modulation coming from the quadratic term of the dielectric interaction.

Another distinctive characteristic is the profile of diffraction peaks under low f ac driving: for LS, the peaks exhibited polarity dependence, where a significantly different diffraction intensity occurs when the driving ac voltage has positive or negative polarity; for NS, each primary diffraction peak is accompanied by a subsequent minor peak, where the phase difference between them depends on f.

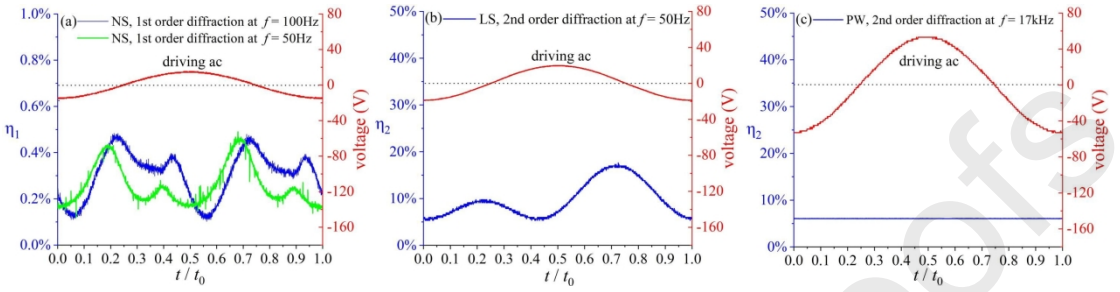

Figure 19. Diffraction dynamics of patterns within a single cycle of the driving ac voltage. (a) Intensity of the 1st order fringe of NS at T = 153 °C, U = 10.5 V, f = 50 Hz and 100 Hz; (b) Intensity of the 2nd order fringe of LS at T = 86 °C, U = 13 V, and f = 50 Hz; (c) Intensity of the 2nd order fringe of PW, at T = 96 °C, U = 39 V, and f = 17 kHz;

4. Applications

With the help of the aforementioned experiments, we observed various self-assembling patterns in 8-F-OH, whose morphologies are changeable under stimuli of electric- or thermal-field. Herein, based on those phenomena, adjustable diffraction grating devices are proposed, whose periodicities can be varied precisely, by utilizing ac voltages of different frequency.

Figure 20 demonstrates the tunability of a device based on the pattern LS, presenting diffraction spots and the corresponding POM snapshots of the pattern. Figure 21 illustrates the similar capabilities of another device utilizing the PW pattern. The current disadvantage of these devices - they operate at elevated temperatures and with low diffraction efficiency- might be overcome in the future with designing proper, new compounds with N_{cybC} phase at lower temperatures, and incorporating

Journal Pre-proofs

more polar group into the structure for larger dipole moment and polarizability.

The efficiency of diffraction on the patterns can be improved by enhancing the modulation of the effective birefringence, which is affected by the sample thickness, the amplitude of the director modulation (tunable by the applied voltage and by adjusting various material parameters like electric anisotropies, elastic moduli, viscosities, flexoelectric coefficients), and the anisotropy of refractive indices (tunable by temperature). As all reported patterns represent nonstandard EC, for which the theoretical background is not fully clear yet, the consequences of adjusting individual parameters is not yet predictable.

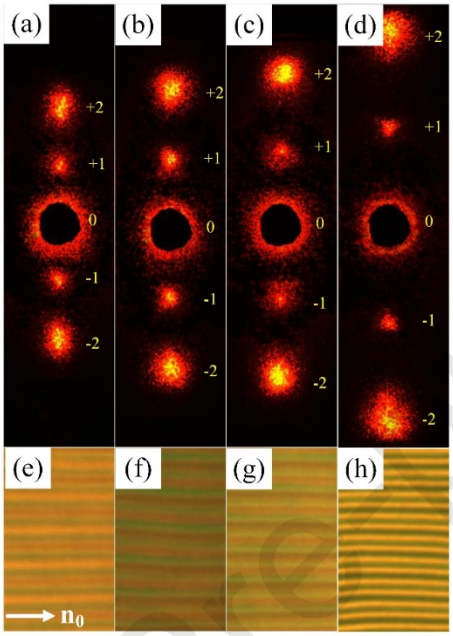

Figure 20. Adjustable diffraction grating based on LS, at fixed T = 79 °C. (a-d) Diffraction fringes under different ac fields, and (e-h) the corresponding pattern morphologies. For (a) $\Lambda \cong 9.4$ μm at U_c= 16 V and f = 40 Hz; (b) $\Lambda \cong 8.5$ μm at U_c = 17.5 V and f = 60 Hz; (c) $\Lambda \cong 7.5$ μm at U_c = 18.8 V and f = 80 Hz; (d) $\Lambda \cong 5.7$ μm at U_c = 24 V and f = 100 Hz.

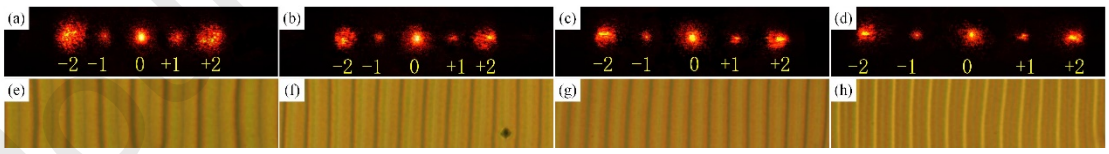

Figure 21. Adjustable diffraction grating based on PW, at fixed T = 105 °C. (a-d) Diffraction fringes under different ac fields, and (e-h) the corresponding pattern morphologies. For (a) $\Lambda \cong 22$ μm at U_c = 49V and f = 50 kHz; (b) $\Lambda \cong 19$ μm at U_c =

Journal Pre-proofs

52 V and f = 55 kHz; (c) $\Lambda \cong$ 15.5 μm at U_c = 58 V and f = 60 kHz; (d) $\Lambda \cong$ 13.5 μm at U_c = 67 V and f = 65 kHz.

5. Discussion

It is well known that LCs are rich in electric-field-induced pattern forming processes assuming proper driving voltage and frequency. Usually, the patterns in nematics appear either due to the flexoelectric effect (flexoelectric domains, FD) or owing to electroconvection effect (EC rolls) [3]. In our case, driven even by very strong dc fields, no patterns were observed, thus we can conclude that compound 8-F-OH has such a combination of its material parameters, which does not allow the occurrence of flexoelectric domains [49].

The results presented above included an in-depth exploration of pattern formation and its dynamics, as well as determination of the polarization state of the diffraction fringes. It has to be noted, however, that the scenarios exhibited in 8-F-OH, and their dependence on temperature, frequency, and voltage, differed in a large extent from the previously reported ones in calamitic nematics as well as in other BCNs. We examined the distinct phenomena in polar nematics and concluded their origins as following:

5.1. The ground state of patterns

For PW, the corresponding ground state is the unperturbed state with uniform texture (pattern free state) at U = 0. Increasing U above U_c, PW grows directly, without experiencing FT. However, in order to produce NS and LS, a FT needs to occur ahead, thus their ground states are the deformed director fields where the director undergoes reorientation upon ac field. Especially, it was observed in planar cell that near the onset of NS, the director aligned almost perpendicular to the surface.

It should be noted that FT appears with two, spatially distributed domains, corresponding to the coexistence of two different deformations, separated by walls. Each of the two FT domains has its own threshold voltage U_F. Increasing the electric field further, NS or LS grow in each of the FT domains independently; consequently, the NS or LS in each FT domain also possess individual critical voltage U_c. Usually, the difference between the two U_c is small, yet there is a situation ($U_{c1} < U < U_{c2}$) where pattern is present in one FT domain only, whereas pattern is absent in the other FT domain. We note that the U_c values presented in Figure 10 correspond to the

Journal Pre-proofs

average of U_{c1} and U_{c2}.

5.2. The structures of patterns

The compound 8-F-OH possesses $\Delta\varepsilon > 0$ and $\Delta\sigma > 0$ at low frequencies where the LS, OS or NS patterns were observed. Nematics with such combination of anisotropies seldom produce patterns. The morphologies reported so far include cellular ones [50-52], localized circular domains (Malthese crosses) [53-55] and fingerprint structures (random stripes) [53]. Recently, normal stripes were reported at high voltages (above the cellular pattern) in 4-cyano-(4'-pentyl)biphenyl (5CB) [51], while longitudinal stripes could also be exerted in the same compound by superposing ac and dc voltages [52]. These patterns are common in that the direct transition from the undistorted state to the patterned one occurs in homeotropic cells; in planar cells pattern formation is preceded by a Fréedericksz transition which provides the necessary conditions for the instability. This scenario is very different from the one found in 8-F-OH, where though the stripes emerge in planar cells after an FT, no patterns arise in homeotropic cells.

One specialty of 8-F-OH is the sign inversion of the dielectric anisotropy at a few kHz. Such a sign inversion in the subMHz range is scarce among nematics, though not unprecedented. So called dual frequency nematics, which possess $\Delta\varepsilon > 0$ below and $\Delta\varepsilon < 0$ above some critical frequency, are known and used in display industry [56-59]. These materials have been designed for displays, thus pattern formation is always prevented. The scenario in 8-F-OH is similar to that in dual frequency nematics: at a fixed T, 8-F-OH has $\Delta\varepsilon > 0$ below and $\Delta\varepsilon < 0$ above the sign inversion frequency. However, at fixed f, $\Delta\varepsilon < 0$ occurs below and $\Delta\varepsilon > 0$ is found above the critical temperature of the sign inversion (Figure 3).

Another specialty in the patterns occurring in 8-F-OH is the continuous variation of the wave vector at low f from longitudinal through oblique to normal stripes upon increasing the temperature. This behavior is quite scarce among pattern forming nematics. Similar pattern transition sequence has previously been reported in the calamitic nematic 4-n-octyloxy-phenyl-4-n'-heptyloxy-benzoate (8/7) with $\Delta\varepsilon < 0$ [59]. It was interpreted as a transition from nonstandard to standard EC upon increasing T, occurring due to the sign inversion of the conductivity anisotropy $\Delta\sigma$, in contrast to the case of 8-F-OH where at low f, $\Delta\varepsilon > 0$ and $\Delta\sigma > 0$ holds in the whole

Journal Pre-proofs

tested N_{cybC} range.

For all the patterns, the induced diffractions are anisotropic, where the diffraction fringes strongly depend on the linearly polarized state $\mathbf{P_{in}}$ of the incident light. It was observed that diffraction occurred only at $\mathbf{P_{in}} \parallel \mathbf{n_0}$ for NS and PW, implying rotation of the director in the *x*-*z* plane, with the wave vector of convection rolls parallel to $\mathbf{n_0}$. However, for LS, the diffraction developed both at $\mathbf{P_{in}} \parallel \mathbf{n_0}$ and $\mathbf{P_{in}} \perp \mathbf{n_0}$, which revealed azimuthal (out of the *x*-*z* plane) rotation of the director, with wave vector of convection rolls perpendicular to $\mathbf{n_0}$.

In addition, this optical anisotropy of the pattern could be proved also by the shadowgraph technique under POM, whose results coincided with that of the anisotropic diffraction.

5.3. The dynamics of patterns

Figure 19(c) demonstrates a near constancy of the intensity diffracted by PW, which reveals that the corresponding director field is stationary, irrespective of the oscillation of the driving ac voltage. Together with the morphologies in Figure 13 and characteristics of the diffraction polarization in Figure 17, it is concluded that PW consists of prewavy-like stripes, similar to the prewavy pattern in traditional BCNs [8].

For NS or LS, while the diffraction intensities still oscillate at 2*f*, like that of the normal or longitudinal rolls in traditional BCNs, they differed significantly in the temporal behavior of the diffraction peaks. The emergence of an additional minor peak in NS (Figure 19(a)) and the polarity dependence of the peak intensity (asymmetric height of the diffraction intensity peaks) in LS (Figure 19(b)) are unexpected.

Typically, an EC pattern is governed by quadratic (proportional to the amplitude square $\mathbf{E}^2$ of the ac field) interactions. Therefore, the EC pattern is expected to be the same in the positive and in the negative half cycle of the applied voltage, and in each half cycle only one diffraction peak should be present.

The polarity dependent asymmetry between half cycles indicates that besides the quadratic one, a linear interaction may also be present. One candidate is flexoelectricity, as taking into account the bent molecular shape, flexoelectricity cannot be excluded as a material property that contributes to the EC scenarios, even

Journal Pre-proofs

though no flexoelectric domains were observed in 8-F-OH. Another source could be the presence of the cybotactic smectic clusters, either via their $\mathbf{P_s}$ or by creating surface polarization.

The presence of a double peak for NS might suggest that two different processes, active in different time slots, govern the formation of the NS pattern. As a paradigm of such possibility, we recall the behavior of the calamitic nematic mixtures Phase 4 and Phase 5 at ultralow frequency driving where the time shifted superposition of standard EC and flexoelectric domains could be observed as alternating patterns [60-62].

Identifying the precise reason of the above mentioned peculiarities of pattern dynamics, nevertheless, require further studies.

6. Conclusion

The novel hockey-stick shaped nematic liquid crystal exhibiting polar properties offer a unique possibility to explore new pattern scenarios. Herein, three kinds of patterns, with distinctive morphology and temporal dynamics, were observed according to appropriate electric- and thermal-field, whose unusual characteristics might be related to the cybotactic nature of the nematic phase.

Besides, the transformations between static Fréedericksz transition and convection patterns were deeply investigated, revealing how a nonlinear system evolves from the equilibrium state with uniform structure to a dynamic state with periodic structure. This issue has seldom been addressed before.

In the end, we had demonstrated tunable diffraction gratings based on self-assembling patterns; nevertheless, how to create more complex patterns in a desired manner still requires further investigations. We expect that the polar nature may provide even more fantastic photonic functionalities.

Acknowledgments

This work was supported by the Guangdong Provincial Science and Technology Plan (Grant No. 2022A1515010777) and the National Natural Science Foundation of China (Grant No. 11774070), the 2018 Inter-Governmental S&T Cooperation Proposal between Hungary and China (8-10, ”Light controlled phenomena in complex

Journal Pre-proofs

fluids", 2018-2.1.14-TÉT-CN-2018-00003), and the grant of the Hungarian National Research, Development and Innovation Office (NKFIH, FK 125134). SKP acknowledges IISER Mohali and SERB Project (CRG/2019/000901/OC). SK acknowledges CSIR (09/947(0254)/2020-EMR-I) for PhD fellowship. GM acknowledges University of Science and Technology Meghalaya, India.

Journal Pre-proofs

References

[1] D. -K. Yang and S. -T. Wu: Fundamentals of Liquid Crystal Devices. John Wiley & Sons Ltd., Chichester, 2006.

[2] Á. Buka, N. Éber, W. Pesch, and L. Kramer: Convective patterns in liquid crystals driven by electric field. In Self-Assembly, Pattern Formation and Growth Phenomena in Nano-Systems. Eds. A. A. Golovin and A. A. Nepomnyashchy, NATO Science Series II, Mathematics, *Physics and Chemistry*, **218**, Springer, Dordrecht, 2006.

[3] N. Éber, P. Salamon and Á. Buka: Electrically induced patterns in nematics and how to avoid them. *Liq. Cryst. Rev*. **4**, 101-134 (2016).

[4] E. Bodenschatz, W. Zimmermann and L. Kramer: On electrically driven pattern-forming instabilities in planar nematics. J. Phys. (Paris) **49**, 1875-1899 (1988).

[5] E. F. Carr: Influence of electric fields on the molecular alignment in the liquid crystal p-(anisalamino)-phenyl acetate. Mol. Cryst. *Liq. Cryst.* **7**, 253-268 (1969).

[6] W. Helfrich: Conduction-induced alignment of nematic liquid crystals: basic model and stability considerations. *J. Chem. Phys.* **51**, 4092-4105 (1969).

[7] A. Krekhov, W. Pesch, N. Éber, T. Tóth-Katona and Á. Buka: Nonstandard electroconvection and flexoelectricity in nematic liquid crystals. *Phys. Rev. E* **77**, 021705 (2008).

[8] J.-H. Huh, Y. Hidaka, Y. Yusril, N. Éber, T. Tóth-Katona, Á. Buka and S. Kai: Prewavy pattern: a director-modulation structure in nematic liquid crystals. *Mol. Cryst. Liq. Cryst*. **364**, 111-122 (2001).

[9] A. Jákli: Liquid crystals of the twenty-first century - Nematic phase of bent-core molecules. *Liq. Cryst. Rev*. **1**, 65-82 (2013).

[10] H. F. Gleeson, S. Kaur, V. Görtz, A. Belaissaoui, S. Cowling and J. W. Goodby: The Nematic Phases of Bent-Core Liquid Crystals. ChemPhysChem **15**, 1251-1260 (2014).

[11] O. Francescangeli,: Samulski, E. T. Insights into the cybotactic nematic phase of bent core molecules. *Soft. Matter.* **6**, 2413-2420(2010).

[12] O. Francescangeli, F. Vita, E. T. Samulski: The cybotactic nematic phase of

Journal Pre-proofs

bent-core mesogens: state of the art and future developments. *Soft. Matter.*,**10**, 7685-7691(2014).

[13] C. Keith, A. Lehmann, U. Baumeister, M. Prehm, C. Tschierske: Nematic phases of bent-core mesogens. *Soft. Matter.*, **6**, 1704-1721(2010).

[14] S. Paladugu, S. Kaur, G. Mohiuddin, R. K. Pujala, S. K. Pal, S. Dhara: Microrheology to probe smectic clusters in bent-core nematic liquid crystals. *Soft. Matter.*, **16**, 7556-7561(2020).

[15] W. Z. Helfrich: The strength of piezoelectricity in liquid crystals. *Z. Naturforsch*. **1971**, *26*, 833-835.

[16] L. Komitov: Molecular Shape Effects in Liquid Crystals. *Mol. Cryst. Liq. Cryst.* 608, 246-257(2015).

[17] P. Sathyanarayana, S. Dhara: Antagonistic flexoelectric response in liquid crystal mixtures of bent-core and rodlike molecules. *Phys. Rev. E: Stat., Nonlinear, Soft .Matter. Phys.* **87**, 012506(2013).

[18] J. Harden,; B. Mbanga, N. Eber, K. Fodor-Csorba, S. Sprunt, J. T. Gleeson, A. Jákli: Giant flexoelectricity of bent-core nematic liquid crystals. *Phys. Rev. Lett.* **97**, 157802(2006).

[19] P. Kumar, Y. G. Marinov, H. P. Hinov, U. S. Hiremath, C. V. Yelamaggad, K. S. Krishnamurthy, A. G. Petrov: Converse Flexoelectric Effect in Bent-Core Nematic Liquid Crystals. *J. Phys. Chem. B* ,**113**, 9168-9174(2009).

[20] P. S. Salter, C. Tschierske, S. J. Elston, E. P. Raynes: Flexoelectric measurements of a bent-core nematic liquid crystal. *Phys. Rev. E*, **84**, 031708(2011).

[21] D. B. Wiant, J. T. Gleeson, N. Éber, K. Fodor-Csorba, A. Jákli and T. Toth-Katona: Non-Standard Electroconvection in a Bent Core Nematic. *Phys. Rev. E* **72**, 041712 (2005).

[22] N. Éber, Á. Buka and K. S. Krishnamurthy: Electrically driven structures in bent-core nematics. *Liq. Cryst*. **49**, 1194-1222(2021).

Journal Pre-proofs

[23] A. Chakraborty, B. Das, M. K. Das, S. Findeisen-Tandel, M.-G. Tamba, U. Baumeister, H. Kresse and W. Weissflog: New hockey stick compounds with a lateral methyl group showing nematic, synclinic and anticlinic smectic C phases. *Liq. Cryst*., **38**, 1085-1097 (2011).

[24] P. Sathyanarayana, S. Radhika, B. K. Sadashiva and S. Dhara: Structure–property correlation of a hockey stick-shaped compound exhibiting N-SmA-SmCa phase transitions. *Soft. Matter* **8**, 2322 (2012).

[25] M. Alaasar, S. Poppe and C. Tschierske: Cybotactic nematic phases of photoisomerisable hockey-stick liquid crystals. *Liq. Cryst.*, **44**, 729-737 (2017).

[26] H. Nishikawa, K. Shiroshita, H. Higuchi, Y. Okumura, Y. Haseba, S. I. Yamamoto, K. Sago, and H. Kikuchi: A Fluid Liquid-Crystal Material with Highly Polar Order. *Adv. Mater*. **29**, 1702354 (2017).

[27] X. Chen, E. Korblova, D. Dong, X. Wei, R. Shao, L. Radzihovsky, M. A. Glaser, J. E. MacLennan, D. Bedrov, D. M. Walba, and N. A. Clark: First-Principles Experimental Demonstration of Ferroelectricity in a Thermotropic Nematic Liquid Crystal: Polar Domains and Striking Electro-Optics. *Proc. Natl. Acad. Sci*. U. S. A. **117**, 14021 (2020).

[28] S. K. Saha, G. Mohiuddin, M. K. Paul, S. P. Gupta, R. K. Khan, S. Ghosh, and S. K. Pal: Polar Switching and Cybotactic Nematic Ordering in 1,3,4-Thiadiazole-Based Short-Core Hockey Stick-Shaped Fluorescent Liquid Crystals. *ACS. Omega* **4**, 7711−7722 (2019).

[29] E-Joon Choi, Hye-Jin Kim, Seung-Chang Kang, Dae-Yoon Kim, Kwang-Un Jeong, You-Jin Lee, Chang-Jae Yu and Jae-Hoon Kim: Polar smectic phases in quasi-bentcore liquid crystals with hockey-stick-shaped mesogen: synthesis and crossover mesomorphism. *Liq. Cryst*., **46**, 2042-2056 (2019).

[30] K. Upadhyaya, S. Ghosh, R. K. Khan, R. Pratibha and N. V. S. Rao: Development of nematic and orthogonal smectic phases in short-core fluorinated hockey-stick shaped liquid crystal compounds. *J. Mol. Liq*. **298**, 111989 (2020).

[31] Unpublished work

[32] S. Kaur, G. Mohiuddin, P. Satapathy, R. Nandi, V. Punjani, S. K. Prasad, S. K.

Journal Pre-proofs

Pal: Influence of terminal halogen moieties on the phase structure of short-core achiral hockey-stick-shaped mesogens: design, synthesis and structure-property relationship. *Mol. Syst. Des. Eng.* **3**, 839-852(2018).

[33] S. Kaur, G. Mohiuddin, V. Punjani, R. K. Khan, S. Ghosh, S. K. Pal: Structural organization and molecular self-assembly of a new class of polar and non-polar four-ring based bent-core molecules. *J. Mol. Liq.* **295**, 111687 (2019).

[34] M. Nagaraj, A. Lehmann, M. Prehm, C. Tschierske, J. K. Vij: Evidence of a polar cybotactic smectic A phase in a new fluorine substituted bent-core compound. *J. Mater. Chem.* **21**, 17098-17103(2011).

[35] G. Shanker, M. Nagaraj, A. Kocot, J. K. Vij, M. Prehm, C. Tschierske,: Nematic phases in 1, 2, 4-Oxadiazole-based bent-core liquid crystals: is there a ferroelectric switching? *Adv. Funct. Mater.* **22**, 1671-1683(2012).

[36] S. Ghosh, N. Begum, S. Turlapati, S. K. Roy, A. K. Das, N. V. S. Rao: Ferroelectric-like switching in the nematic phase of four-ring bent-core liquid crystals. *J. Mater. Chem. C* **2**, 425-431(2014).

[37] G. Shanker, M. Prehm,; M. Nagaraj, J. K. Vij, M. Weyland, A. Eremin, C. Tschierske: 1,2,4-Oxadiazole-Based Bent-Core Liquid Crystals with Cybotactic Nematic Phases. *ChemPhysChem* **15**, 1323-1335(2014).

[38] A. Krekhov, W. Decker, W. Pesch, N. Éber, P. Salamon, B. Fekete, and Á. Buka: Patterns driven by combined ac and dc electric fields in nematic liquid crystals. *Phys. Rev. E* **89**, 052507 (2014).

[39] N. Éber, P. Salamon, B. A. Fekete, R. Karapinar, A. Krekhov, and Á. Buka: Suppression of spatially periodic patterns by dc voltage. *Phys. Rev. E* **93**, 042701 (2016).

[40] W. Pesch, A. Krekhov: Optical analysis of spatially periodic patterns in nematic liquid crystals: Diffraction and shadowgraphy. *Phys. Rev. E* **87**, 52504 (2013).

[41] Y, Xiang, H. Z. Jing, Z. D. Zhang, W. J. Ye, M. Y. Xu, E. Wang, P. Salamon, N. Éber, and Á. Buka: Tunable optical grating based on the flexoelectric effect in a

Journal Pre-proofs

bent-core nematic liquid crystal. *Phys. Rev. Appl.* **7,** 064032 (2017).

[42] N. Éber, S. A. Rozanski, S. Németh, Á. Buka, W. Pesch, L. Kramer: Decay of spatially periodic patterns in a nematic liquid crystal. *Phys. Rev.* **E** , **70**, 061706/1-8 (2004).

[43] W. Pesch, L. Kramer, N. Éber, Á. Buka: The Role of Initial Conditions in the Decay of Spatially Periodic Patterns in a Nematic Liquid Crystal. *Phys. Rev. E*, **73**, 061705/1-10 (2006).

[44] E. Bodenschatz, W. Pesch, L. Kramer: Structure and dynamics of dislocations in anisotropic pattern forming systems, Physica D 32, 135–145 (1988).

[45] S. Nasuno, S. Takeuchi, Y. Sawada: Motion and interaction of dislocations in electrohydrodynamic convection of nematic liquid crystals. *Phys. Rev. A* **40**, 3457–3460 (1989).

[46] A. L. Susser, S. Kralj and C. Rosenblatt: Co-revolving topological defects in a nematic liquid crystal. *Soft. Matter* **17**, 9616 (2021).

[47] Y. Xiang, H. Z Jing, W. Y. Sun, H. Chen, G. Cipparrone, P. Pagliusi, M.Y. Xu, G.H. Huang, E. Wang: Topological defects arrays and control of electro-convections in periodically photo-aligned bent-core nematics. *J. Mol. Liq.* **318**,114058(2020).

[48] Y. Xiang, H. Z Jing, H. Chen, J. Zhang, X.Y. Ding , J. Y. Li, Z. Z. Cai, N. Éber , Á. Buka: Light-driven rotation of gratings formed by electroconvection patterns in cholesteric liquid crystals，*J. Mol. Liq.***337**,116366 (2021).

[49] A. Krekhov, W. Pesch, Á. Buka: Flexoelectricity and pattern formation in nematic liquid crystals. *Phys. Rev. E* **83**, 51706 (2011).

[50] M. Nakagawa and T. Akahane: A New Type of Electrohydrodynamic Instability in Nematic Liquid Crystals with Positive Dielectric Anisotropy. I. The Existence of the Charge Injection and the Diffusion Current. *J. Phys. Soc. Jpn*. **52**, 3773-3782 (1983).

[51] P. Kumar, J. Heuer, T. Tóth-Katona, N. Éber, and Á. Buka: Convection-roll instability in spite of a large stabilizing torque. *Phys. Rev. E* **81**, 020702(R) (2010).

[52] L. E. Aguirre, E. Anoardo, N. Éber and Á. Buka: Regular structures in 5CB liquid crystals under the joint action of ac and dc voltages. *Phys. Rev. E* **85**, 041703

Journal Pre-proofs

(2012).

[53] M. I. Barnik, L. M. Blinov, S. A. Pikin, and A. N. Trufanov: Instability mechanism in the nematic and isotropic phases of liquid crystals with positive dielectric anisotropy. *Sov. Phys. JETP* **45**, 396 (1977).

[54]A. N. Trufanov, M.I. Barnik, L.M. Blinov, V.G. Chigrinov: Electrohydrodynamic instability in homeotropically oriented layers of nematic liquid crystals. *Zh. Eksp. Teor. Fiz*. **80**, 704 (1981).

[55] D. K. Rout and R. N. P. Choudhary: Electrohydrodynamic instability in some nematic cyanobiphenyls in an a.c. electric field. *Liq. Cryst.* **4**, 393 (1989).

[56] A. B. Golovin, S. V. Shiyanovskii, and O. D. Lavrentovich: Fast switching dual-frequency liquid crystal optical retarder, driven by an amplitude and frequency modulated voltage. *Appl. Phys. Lett*. **83**(19), 3864–3866 (2003).

[57] X.-W. Lin, W. Hu, X.-K. Hu, X. Liang, Y. Chen, H.-Q. Cui, G. Zhu, J.-N. Li, V. Chigrinov, and Y.-Q. Lu: Fast response dual-frequency liquid crystal switch with photo-patterned alignments. *Opt. Lett*. **37**(17), 3627–3629 (2012).

[58] M. Mrukiewicz, P. Perkowski, W. Piecek, R. Mazur, O. Chojnowska, and K. Garbat: Two-step switching in dual-frequency nematic liquid crystal mixtures. *J. Appl. Phys.* **118**(17), 173104 (2015).

[59] T. Tóth-Katona, A. Cauquil-Vergnes, N. Éber, Á. Buka: Non-standard electroconvection with Hopf-bifurcation in a nematic with negative electric anisotropies. *Phys. Rev. E*, **75**, 066210/1-12 (2007).

[60] M. May, W. Schöpf, I. Rehberg, A. Krekhov, A. Buka: Transition from longitudinal to transversal patterns in an anisotropic system. *Phys. Rev. E* **78**, 46215 (2008).

[61] N. Éber, L.O. Palomares, P. Salamon, A. Krekhov and Á. Buka: Temporal evolution and alternation of mechanisms of electric field induced patterns at ultra-low-frequency driving. *Phys. Rev. E* **86**, 021702/1-9 (2012).

[62] P. Salamon, N. Éber, A. Krekhov, Á. Buka: Flashing flexodomains and electroconvection rolls in a nematic liquid crystal. *Phys. Rev. E* **87**, 032505 (2013).

Journal Pre-proofs

- Electroconvective phenomena were observed in cybotactic nematics, demonstrating ferroelectric-like switching behaviors.
- Patterns with different morphologies can be selected by temperature and driving frequency.
- Patterns were ascribed to the strongly deformed boundary layers.

Conflict of Interests:

All authors have no conflict of interest.

Author 1 (First Author): Investigation, Formal Analysis, Writing - Original Draft;

Author 2(Corresponding Author): Conceptualization, Funding Acquisition, Resources, Supervision, Writing - Review & Editing. Data Curation, Writing - Original Draft;

Author 3: Visualization, Investigation;

Author 4: Conceptualization, Resources;

Author 5: Conceptualization, Methodology, Investigation,

Author 6: Visualization, Writing - Review & Editing

Journal Pre-proofs

Author 7 (Corresponding Author): Conceptualization, Funding Acquisition, Resources, Supervision, Writing - Review & Editing. Data Curation, Writing - Original Draft;

Author 8 (Corresponding Author): Conceptualization, Funding Acquisition, Resources, Supervision, Writing - Review & Editing. Data Curation, Writing - Original Draft;

Author 9：Conceptualization, Methodology, Review & Editing

Author 10：Conceptualization, Methodology, Review & Editing

Journal Pre-proofs